JOURNAL OF GUIDANCE, CONTROL, AND DYNAMICS
Vol. 30, No. 6, November–December 2007

Modeling and Simulation of Airship Dynamics

Yuwen Li* and Meyer Nahon†
McGill University, Montreal, Quebec H3A 2K6, Canada

DOI: 10.2514/1.29061

This paper proposes a modeling approach for the nonlinear dynamics simulation of airships. The flight mechanics, aerostatics, and aerodynamics are incorporated into the model. A comprehensive estimation method is provided for the aerodynamics, including added-mass terms, viscous effect, forces on the fins, forces on the hull due to the fins, and axial drag. A simulation program is developed from the dynamics model and applied to analyze the control responses of the Skyship-500 airship. A comparison between the simulation and flight test results for different control inputs shows that the dynamics simulation gives a reasonable estimation of the flight behavior. The dynamics model is then linearized using a finite difference approach and the linear model is applied to investigate the stability of longitudinal and lateral motion at various speeds. With the trust gained from validation, the dynamics model and simulation program can be used to evaluate the flight and control performance of other airships.

Nomenclature

$\mathbf{A}$, $\mathbf{B}$	=	state matrix and input matrix of the linear model, respectively
b	=	fin semispan
C_D, C_L, C_M	=	drag, lift, and pitching moment coefficients
C_{DH0}, C_{DF0}	=	zero-angle axial drag coefficients of hull and fins, respectively
$C_{L\alpha}$, $C_{l\alpha}$	=	3-D and 2-D lift curve slopes of the fins
c, c_f	=	airfoil chord and flap chord
$\mathbf{F}_G$, $\mathbf{F}_{\mathrm{AS}}$	=	force vectors due to gravity and aerostatics, respectively
$F_{\mathrm{NF}}(F_{yF}, F_{zF})$	=	normal forces (in y and z directions) acting on a fin
$F_{\mathrm{NH}(F)}$	=	normal forces acting on the hull due to the fins
$F_{\mathrm{NV}}(F_{yV}, F_{zV})$	=	normal forces (in y and z directions) due to viscosity on the hull
g	=	acceleration of gravity
$\mathbf{J}$	=	inertia tensor of the airship
k_1, k_2, k'	=	added-mass factors of ellipsoids
$k_{3\text{-D}}$	=	3-D efficiency factor for the aerodynamics of control surface deflection
k_{44}	=	body-fin factor
$\mathbf{M}$	=	mass matrix of the airship
$\mathbf{M}_A$, $\mathbf{M}_{\mathrm{AH}}$, $\mathbf{M}_{\mathrm{AF}}$	=	added-mass matrices of the airship, the hull, and the fins, respectively
M_{xF}, M_{yF}, M_{zF}	=	rolling, pitching, and yawing moments from F_{NF}
M_{yV}, M_{zV}	=	pitching and yawing moments from F_{NV}
m	=	total mass of the airship
m_{Hij}, m_{Fij}	=	elements of added-mass matrices $\mathbf{M}_{\mathrm{AH}}$ and $\mathbf{M}_{\mathrm{AF}}$, respectively
m_{22}^{SF}, m_{33}^{SF}, m_{44}^{SF}	=	cross-sectional added mass and moment of inertia of the fins
m', I'	=	mass and moment of inertia of the air displaced by the hull
$q_0 = 1/2\rho V^2$	=	dynamic pressure
R	=	hull cross-sectional radius
$\mathbf{r}_g$, $\mathbf{r}_v$	=	position vectors of the CG and CV from the body-frame origin
S	=	hull cross-sectional area
S_f, S_{FA}	=	flap and fin area, respectively
S_H, S_F	=	reference areas for the axial drag of the hull and the fins, respectively
s	=	spanwise position
$\mathbf{U}_e$, $\Delta\mathbf{U}$	=	equilibrium control input and disturbance in control input
u_e	=	equilibrium speed
V	=	airspeed
V_B	=	airship volume
$\mathbf{v} = [u, v, w]^T$	=	linear velocity vector
v_n, v_t	=	local velocity perpendicular and parallel to the fin surface, respectively
w_d	=	downwash due to the fins
$\mathbf{X}_e$, $\Delta\mathbf{X}$	=	equilibrium state vector and disturbance in state vector
x, y, z	=	coordinates of a point in the body frame
x_{fs}, x_{fe}	=	x coordinates of the start and the end positions of the fins
α_F, α_e	=	geometric and effective angles of attack of the fins
γ	=	angle between centerline and velocity vector
$\Delta C_{p\alpha}$	=	$\partial \Delta C_p / \partial \alpha$, where ΔC_p is the pressure coefficient of the airfoil
δ_E, δ_R	=	elevator and rudder deflection, respectively
ε	=	longitudinal distance from the nose
η	=	efficiency factor for the crossflow drag due to the finite length
η_d	=	correction factor for the flap effectiveness factor
η_f	=	efficiency factor for the fin added mass due to 3-D effect
$\lambda_{1,2} = \sigma \pm \mathrm{j}\omega_d$	=	eigenvalues
ρ	=	air density
τ	=	theoretical flap effectiveness factor
$\boldsymbol{\tau}_{\mathrm{AS}}$, $\boldsymbol{\tau}_A$	=	forces and moments from aerostatics and added mass, respectively
$\boldsymbol{\tau}_I$, $\boldsymbol{\tau}_G$, $\boldsymbol{\tau}_C$	=	forces and moments from inertia, gravity, and control, respectively
Φ_F	=	angle from the oxz plane to the fin surface plane
ϕ, θ, ψ	=	Euler angles
$\boldsymbol{\omega} = [p, q, r]^T$	=	angular velocity vector

Presented as Paper 6618 at the AIAA Modeling and Simulation Technologies Conference and Exhibit, Keystone, Colorado, 21–24 August 2006; received 28 November 2006; revision received 25 March 2007; accepted for publication 3 April 2007.

*Ph.D. Student, Department of Mechanical Engineering, 817 Sherbrooke Street West; liyuwen@cim.mcgill.ca. Student Member AIAA.

†Associate Professor, Department of Mechanical Engineering, 817 Sherbrooke Street West; Meyer.Nahon@mcgill.ca. Associate Fellow AIAA.

I. Introduction

IN THE past few years, researchers have become increasingly interested in airships, because these aircraft can provide long endurance, high payload-to-weight ratio, and low fuel consumption [1–4]. The resurgence of airships has created a need for accurate dynamics models and simulation capabilities to analyze their flight behavior and to design their control systems.

A number of textbooks, such as [5], have derived the equations of motion for conventional aircraft, for which certain solid–fluid interaction forces can be neglected, such as buoyancy and those related to the inertia of the surrounding air. However, these forces become important for airships because their flight relies on a light lifting gas rather than aerodynamic lift forces. This distinguishing feature implies that their dynamics models must include a more complete formulation for the interaction forces between the body and the air. A number of airship models have been presented in the literature. Tischler et al. [6] derived the nonlinear equations of motion and developed the simulation program HLASIM for the design of heavy lift airships; Jex and Gelhausen [7] applied their model and frequency-domain fitting technique to predict the control responses of the Skyship-500 airship. Amann [8] followed the aerodynamics prediction method of Jones and DeLaurier [9] and developed a dynamic simulation program to analyze the flight characteristics, also for the Skyship-500. Azinheira et al. [10] investigated how to incorporate the wind effects into the nonlinear equations of motion of airships. Cook et al. [11] formulated the linearized equations of motion for airship stability analysis. Such analytical linear dynamics models with aerodynamic stability derivatives usually neglect the nonlinear effects, but have the advantage that they can be readily improved by updating the aerodynamic derivatives obtained from wind-tunnel or flight tests. On the other hand, in case such experimental tests are not possible, a reasonable aerodynamic prediction approach can be very useful. Another important limitation of the above airship dynamics models is that relatively little detail is given on the aerodynamic force estimation. Furthermore, most of these models have not been validated by actual flight test results.

In this paper, a modeling approach is proposed to assemble the nonlinear equations of motion for the simulation of airship dynamics, with a particular focus on a comprehensive formulation of the interaction forces between the airship and the air and on the model validation. For this purpose, the derivation begins from the equations of motion of a rigid-body vehicle moving in vacuum in Sec. II. Then the relevant solid–fluid interaction forces, both aerostatics and aerodynamics, are incorporated into the equations in Secs. III and IV. A linearization procedure is discussed in Sec. V to obtain the linear equations of motion. In Sec. VI, the nonlinear dynamics model is used to simulate the Skyship-500 airship and the linearized model is applied to investigate its stability.

II. Equations of Motion for Airship in Vacuum

The modeling begins from the simplest case of a rigid-body airship moving in vacuum. For convenience, the equations of motion for a 6-DOF (degrees of freedom) vehicle are usually derived in a body frame $\{oxyz\}$ (shown in Fig. 1), which can be located at an arbitrary position without loss of generality. For a body moving in vacuum, these equations have been derived in standard textbooks [5,12] using the Newton–Euler approach, and can be summarized in vector form as

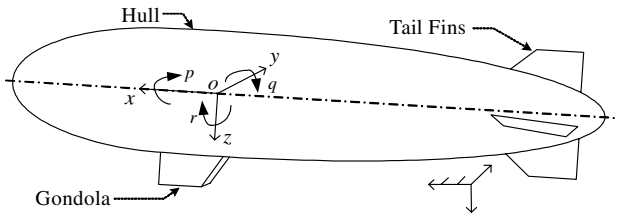

Fig. 1 Body frame.

$$\mathbf{M}\dot{\mathbf{V}} = \boldsymbol{\tau}_I + \boldsymbol{\tau}_G + \boldsymbol{\tau}_C \tag{1}$$

where $\mathbf{V} = [\mathbf{v}^T, \boldsymbol{\omega}^T]^T$, and $\mathbf{v} = [u, v, w]^T$ and $\boldsymbol{\omega} = [p, q, r]^T$ denote the linear and angular velocity vectors expressed in the body frame, respectively. $\mathbf{M}$ is the mass matrix of the body and can be written as

$$\mathbf{M} = \begin{bmatrix} m\mathbf{I}_{3\times 3} & -m\mathbf{r}_g^{\times} \\ m\mathbf{r}_g^{\times} & \mathbf{J} \end{bmatrix} \tag{2}$$

where m is the total mass, including the hull, gas, gondola, fins, ballonets, etc. $\mathbf{J}$ is the inertia tensor, and $\mathbf{r}_g$ is the position vector of the center of gravity (CG) from the origin o. Note that $\mathbf{J}$ and $\mathbf{r}_g$ are both expressed in the body frame. The superscript $\times$ denotes the skew-symmetric matrix form of a vector (corresponding to a cross-product operation).

The right-hand side of Eq. (1) consists of the external forces and moments. The subscripts I, G, and C denote the terms from inertia, gravity, and control, respectively. The inertial and gravity forces and moments are calculated as

$$\boldsymbol{\tau}_I = \begin{bmatrix} -m\boldsymbol{\omega}^{\times}\mathbf{v} + m\boldsymbol{\omega}^{\times}\mathbf{r}_g^{\times}\boldsymbol{\omega}^{\times} \\ -m\mathbf{r}_g^{\times}\boldsymbol{\omega}^{\times}\mathbf{v} - \boldsymbol{\omega}^{\times}\mathbf{J}\boldsymbol{\omega} \end{bmatrix}, \qquad \boldsymbol{\tau}_G = \begin{bmatrix} \mathbf{F}_G \\ \mathbf{r}_g^{\times}\mathbf{F}_G \end{bmatrix} \tag{3}$$

where $\mathbf{F}_G = mg[-\sin\theta, \cos\theta\sin\phi, \cos\theta\cos\phi]^T$, in which g is the acceleration of gravity and ϕ, θ, and ψ are Euler angles. If the body frame is located at the CG, $\mathbf{r}_g = \mathbf{0}$ and the terms related to $\mathbf{r}_g$ will be zero.

The control force and moment $\boldsymbol{\tau}_C$ are due to the thruster, the deflection of control surfaces, and the inflation or deflation of ballonets, and are generated by the automatic control system or the pilot's commands. Some of these forces are generated aerodynamically, such as the control surface deflection, and will be discussed in Sec. IV.

III. Interaction Forces and Moments Between Airship and Air: Aerostatics

We can now start to incorporate the interaction forces and moments between the vehicle and the air, which include two components: aerostatics and aerodynamics. The former is due to the static air pressure and is independent of the motion of the body while the latter is related to its motion.

If the position vector of the center of volume (CV) relative to the origin o is $\mathbf{r}_v$, then the aerostatic force and moment expressed in the body frame is

$$\boldsymbol{\tau}_{\mathrm{AS}} = \begin{bmatrix} \mathbf{F}_{\mathrm{AS}} \\ \mathbf{r}_v^{\times}\mathbf{F}_{\mathrm{AS}} \end{bmatrix} \tag{4}$$

where $\mathbf{F}_{\mathrm{AS}} = -\rho g V_B[-\sin\theta, \cos\theta\sin\phi, \cos\theta\cos\phi]^T$, in which V_B is the volume of the body, while ρ is the air density. If the body frame is established at the CV, $\mathbf{r}_v = \mathbf{0}$ and the aerostatic moment is zero. To incorporate the aerostatics into the equations of motion, $\boldsymbol{\tau}_{\mathrm{AS}}$ is added to the right-hand side of Eq. (1).

IV. Interaction Forces and Moments Between Airship and Air: Aerodynamics

The aerodynamic forces are categorized into various terms based on different physical effects. Estimation methods for each of these terms are now investigated.

A. Added-Mass Force and Moment

1. Added-Mass Force and Moment Computation from the Added-Mass Matrix

The added-mass force and moment can be considered as the pressure-induced fluid-structure interaction terms based on the potential flow assumption [12]. For a body completely submerged in an unbounded fluid, the added-mass terms can be derived by an energy approach in terms of Kirchhoff's equations [12,13] or alternatively by using Bernoulli's equation to find the pressure

distribution over the body [14]. Here we will not repeat the detailed derivation but just review the results. That is, the symmetric added-mass matrix is written as

$$\mathbf{M}_A = \begin{bmatrix} \mathbf{M}_{11} & \mathbf{M}_{12} \\ \mathbf{M}_{21} & \mathbf{M}_{22} \end{bmatrix} \tag{5}$$

where $\mathbf{M}_{11}$, $\mathbf{M}_{12}$, $\mathbf{M}_{21}$, and $\mathbf{M}_{22}$ are 3×3 submatrices, whose elements can be estimated using the methods discussed in Sec. IV.A.2. The corresponding added-mass force and moment can be obtained in vector form as

$$\boldsymbol{\tau}_A = -\begin{bmatrix} \mathbf{M}_{11} & \mathbf{M}_{12} \\ \mathbf{M}_{21} & \mathbf{M}_{22} \end{bmatrix} \begin{bmatrix} \dot{\mathbf{v}} \\ \dot{\boldsymbol{\omega}} \end{bmatrix} - \begin{bmatrix} \boldsymbol{\omega}^{\times}(\mathbf{M}_{11}\mathbf{v} + \mathbf{M}_{12}\boldsymbol{\omega}) \\ \mathbf{v}^{\times}(\mathbf{M}_{11}\mathbf{v} + \mathbf{M}_{12}\boldsymbol{\omega}) + \boldsymbol{\omega}^{\times}(\mathbf{M}_{21}\mathbf{v} + \mathbf{M}_{22}\boldsymbol{\omega}) \end{bmatrix} \tag{6}$$

Thus $\boldsymbol{\tau}_A$ includes two terms: one related to the time rates of change of the linear and angular velocities, the other related to the coupling of the linear and angular velocities. Note that for an airship in steady translation, only the moment term $-\mathbf{v}^{\times}(\mathbf{M}_{11}\mathbf{v})$ appears in Eq. (6), which is known as the Munk moment [15], and tends to destabilize the pitch or yaw motion. To incorporate the added-mass force and moment into the dynamics model, the first term in Eq. (6) is written on the left-hand side of Eq. (1) so that the mass matrix $\mathbf{M}$ is replaced by $\mathbf{M} + \mathbf{M}_A$, while the second term is added to the right-hand side of Eq. (1).

2. *Estimation of the Added-Mass Matrix*

The total added-mass matrix of the airship includes the contributions of both the hull and the fins, that is,

$$\mathbf{M}_A = \mathbf{M}_{\mathrm{AH}} + \mathbf{M}_{\mathrm{AF}} \tag{7}$$

In practice, a simple approach to obtain the added mass and moment of inertia of the hull $\mathbf{M}_{\mathrm{AH}}$ is to approximate the hull as an ellipsoid of revolution. If the body frame is located at the CV, with the x axis along the centerline and positively toward the nose and the z axis positively downward, then all the off-diagonal terms in the added-mass matrix of the hull are zero and the diagonal terms are

$$\begin{aligned} m_{H11} &= k_1 m', \qquad m_{H22} = m_{H33} = k_2 m' \\ m_{H44} &= 0, \qquad m_{H55} = m_{H66} = k' I' \end{aligned} \tag{8}$$

where m' is the mass of air displaced by the hull and I' is the moment of inertia of the displaced air. k_1, k_2, and k' are added-mass factors [12] plotted in Fig. 2 as functions of the fineness ratio L/D, where L is the length of the hull and D is its maximum diameter.

The added mass and moment of inertia of the fins can be computed by integrating the 2-D added mass of the cross section over the fin region. For example, for the cross section with cruciform fins shown in Fig. 3, the 2-D transverse added mass in the y and z directions, and the added moment of inertia about the x axis can be computed using potential flow theory as discussed in [16]. The contribution of the fins to these 2-D added-mass terms can be written as

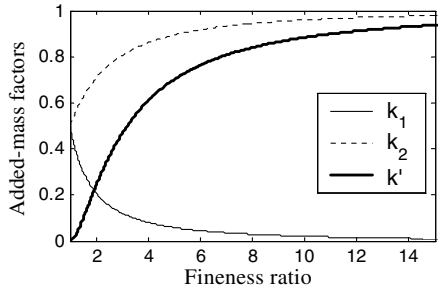

Fig. 2 Added-mass factors.

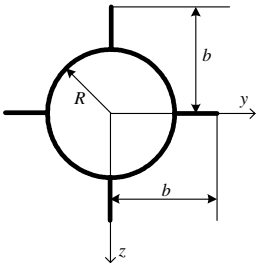

Fig. 3 Fin cross section.

$$m_{22}^{\mathrm{SF}} = m_{33}^{\mathrm{SF}} = \rho\pi(b - R^2/b)^2, \qquad m_{44}^{\mathrm{SF}} = 2k_{44}\rho b^4/\pi \tag{9}$$

where R is the body cross-sectional radius and b is the fin semispan. The factor k_{44} is plotted in Fig. 4 as a function of R/b. The 2-D added mass of cross sections with other fin arrangements can be also found in [16].

The nonzero elements in the added-mass matrix of the fins $\mathbf{M}_{\mathrm{AF}}$ are obtained by integrating Eq. (9) over the fin region, that is,

$$\begin{aligned} m_{F22} = m_{F33} = \eta_f \int_{x_{fs}}^{x_{fe}} m_{22}^{\mathrm{SF}}\,\mathrm{d}x, \qquad m_{F35} = -\eta_f \int_{x_{fs}}^{x_{fe}} m_{22}^{\mathrm{SF}} x\,\mathrm{d}x \\ m_{F26} = -m_{F35}, \qquad m_{F44} = \eta_f \int_{x_{fs}}^{x_{fe}} m_{44}^{\mathrm{SF}}\,\mathrm{d}x \\ m_{F55} = m_{F66} = \eta_f \int_{x_{fs}}^{x_{fe}} m_{22}^{SF} x^2\,\mathrm{d}x \end{aligned} \tag{10}$$

where x_{fs} and x_{fe} are the x coordinates of the start and end positions of the fins. An efficiency factor η_f (shown in Fig. 5) is included to account for 3-D effects; it is calculated from potential flow theory for the added mass of a thin plate [17,18] and determined based on the aspect ratio.

B. Viscous Effect on the Hull, Normal to the Centerline

Wind-tunnel tests on the aerodynamics of bodies of revolution at angles of attack have shown that a prediction based on potential flow assumption can cause considerable error because of the effects of viscosity, especially at the rear of the body. Finck and Hopkins in

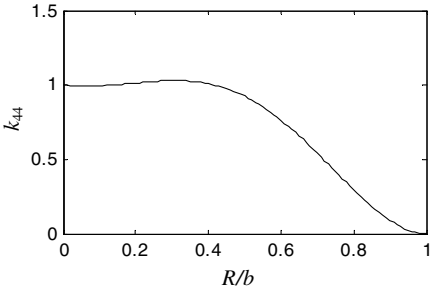

Fig. 4 Body-fin factor k_{44}.

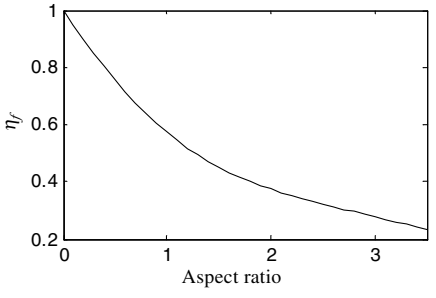

Fig. 5 Efficiency factor η_f.

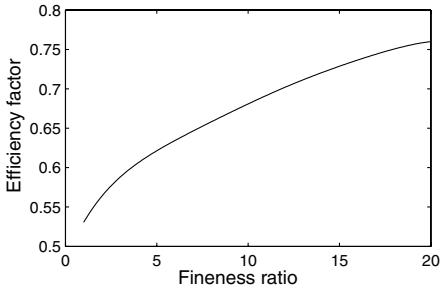

Fig. 6 Efficiency factor η.

[19,20] give a semi-experimental estimation approach for the aerodynamics of bodies of revolution; in this approach, the force normal to the centerline due to viscous effects can be computed as

$$F_{\mathrm{NV}} = -q_0 \sin 2\gamma \cdot (k_2 - k_1) \int_{\varepsilon_0}^{L} (\mathrm{d}S/\mathrm{d}\varepsilon)\, \mathrm{d}\varepsilon + q_0 \eta C_{\mathrm{DC}} \sin^2\gamma \cdot \int_{\varepsilon_0}^{L} 2R\, \mathrm{d}\varepsilon \tag{11}$$

where C_{DC} is the crossflow drag coefficient of an infinite-length circular cylinder, η is an efficiency factor accounting for the finite length of the body and determined from the fineness ratio of the body (shown in Fig. 6), R and S are the local cross-sectional radius and area, ε denotes the longitudinal position from the nose and ε_0, the location at which the flow ceases to be potential, is empirically determined as [20]

$$\varepsilon_0 = 0.378L + 0.527\varepsilon_1$$

where ε_1 denotes the position at which $\mathrm{d}S/\mathrm{d}\varepsilon$ has a maximum negative value. The dynamic pressure q_0 and the angle between the centerline and the velocity vector γ (shown in Fig. 7) is computed from the local velocity (u_V, v_V, w_V) at the position ε_0, that is,

$$\gamma = \tan^{-1}\left(\sqrt{v_V^2 + w_V^2}/u_V \right) \tag{12}$$

The first term in Eq. (11) effectively removes the inviscid flow contribution downstream of ε_0 while the second term replaces it with a viscous flow contribution. F_{NV} can be further decomposed into

$$F_{yV} = -F_{\mathrm{NV}} \cdot v_V / \sqrt{v_V^2 + w_V^2}, \qquad F_{zV} = -F_{\mathrm{NV}} \cdot w_V / \sqrt{v_V^2 + w_V^2} \tag{13}$$

The corresponding moment about the origin of the body frame is computed as

$$M_V = -q_0 \sin 2\gamma \cdot (k_2 - k_1) \int_{\varepsilon_0}^{L} \mathrm{d}S/\mathrm{d}\varepsilon (\varepsilon_m - \varepsilon)\, \mathrm{d}\varepsilon + q_0 \eta C_{\mathrm{DC}} \sin^2\gamma \cdot \int_{\varepsilon_0}^{L} 2R(\varepsilon_m - \varepsilon)\, \mathrm{d}\varepsilon \tag{14}$$

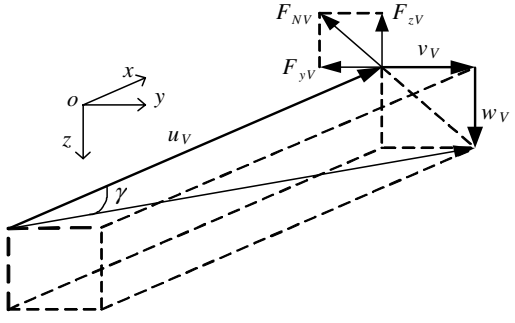

Fig. 7 Normal force decomposition.

where ε_m is the position of the origin of the body frame from the nose. The pitching and yawing moments are obtained from M_V as

$$M_{yV} = M_V \cdot w_V / \sqrt{v_V^2 + w_V^2}, \qquad M_{zV} = -M_V \cdot v_V / \sqrt{v_V^2 + w_V^2} \tag{15}$$

Equations (13) and (15) are applied to compute the normal forces due to viscosity on the hull and the corresponding moments. These forces and moments are then added to the right-hand side of Eq. (1).

C. Force Acting on the Fins, Normal to the Centerline

We now turn our attention to the force produced by the fins, normal to the airship centerline. This is obtained by estimating the force distribution and integrating this over the fin area. If we consider a point P on the fin planform (shown in Fig. 8), with longitudinal position x and spanwise position s, the normal force at an area element is predicted as

$$dF_{\mathrm{NF}} = q_0 \Delta C_{p\alpha}(x, s) \alpha_e(x, s)\, \mathrm{d}x\, \mathrm{d}s \tag{16}$$

where $\Delta C_{p\alpha} \equiv \partial \Delta C_p / \partial \alpha$, and ΔC_p is the pressure coefficient of the airfoil; $\Delta C_{p\alpha}$ is determined by the local chordwise position and can be obtained from experiments or from CFD (computational fluid dynamics) results of the pressure distribution of the airfoil. α_e is the effective angle of attack computed as

$$\alpha_e = C_{L\alpha}/C_{l\alpha} \cdot (1 + R^2/s^2) \cdot \alpha_F \tag{17}$$

where $C_{L\alpha}/C_{l\alpha}$ is a correction factor for 3-D effects and can be obtained from finite wing theories, such as those in [21]. The factor $(1 + R^2/s^2)$ accounts for the influence of the hull on the fins [22]. α_F is the geometric angle of attack computed from the local velocity at the center of the 1/4 chord. Figure 9 shows a fin located in the plane inclined at an angle Φ_F from the oxz plane. The velocity component in the x direction at its center of the 1/4 chord is u_F and the transverse velocity is decomposed into v_n, perpendicular to the fin surface, and v_t, parallel to the surface. Then the geometric angle of attack is computed as

$$\alpha_F = \tan^{-1}(v_n/u_F) \tag{18}$$

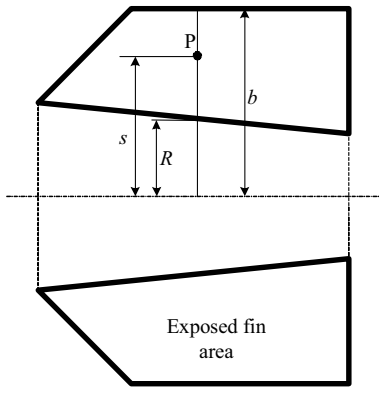

Fig. 8 Fin planform.

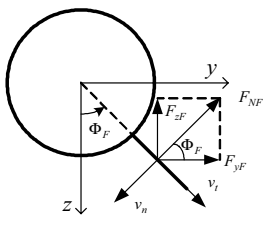

Fig. 9 Normal force on a fin.

If α_F is beyond the angle α_{stall} at which the stall occurs, we use α_{stall} to calculate the effective angle of attack in Eq. (17). The value of α_{stall} can be estimated by the methods in [19]. The total normal force on the fin is obtained by integrating the force distribution, from Eq. (16), over the exposed fin area, and then decomposed into F_{yF} and F_{zF}, that is,

$$F_{yF} = F_{\text{NF}} \cos \Phi_F, \qquad F_{zF} = -F_{\text{NF}} \sin \Phi_F \tag{19}$$

where

$$F_{\text{NF}} = q_0 (C_{L\alpha}/C_{l\alpha}) \alpha_F \int_{x_{fs}}^{x_{fe}} \int_R^b \Delta C_{p\alpha}(x, s)(1 + R^2/s^2)\, \mathrm{d}s\, \mathrm{d}x$$

The corresponding rolling, pitching, and yawing moments on the fin are

$$\begin{aligned} M_{xF} &= -q_0 (C_{L\alpha}/C_{l\alpha}) \alpha_F \int_{x_{fs}}^{x_{fe}} \int_R^b s \Delta C_{p\alpha}(x, s)(1 + R^2/s^2)\, \mathrm{d}s\, \mathrm{d}x \\ M_{yF} &= q_0 \sin \Phi_F (C_{L\alpha}/C_{l\alpha}) \alpha_F \\ &\quad \times \int_{x_{fs}}^{x_{fe}} \int_R^b x \Delta C_{p\alpha}(x, s)(1 + R^2/s^2)\, \mathrm{d}s\, \mathrm{d}x, \\ M_{zF} &= q_0 \cos \Phi_F (C_{L\alpha}/C_{l\alpha}) \alpha_F \\ &\quad \times \int_{x_{fs}}^{x_{fe}} \int_R^b x \Delta C_{p\alpha}(x, s)(1 + R^2/s^2)\, \mathrm{d}s\, \mathrm{d}x \end{aligned} \tag{20}$$

Equations (19) and (20) can be applied to compute the normal forces and corresponding moments on each fin, which are then added to the right-hand side of Eq. (1).

D. Force Acting on the Hull Due to the Fins, Normal to the Centerline

Based on the results from wind-tunnel tests on the aerodynamics of airships, such as the Akron [23,24], it has been found that the presence of the fins can lead to extra normal force on the hull, due to the fin-induced downwash over the airflow near the hull. The extra normal force per unit length on the hull can be obtained as [25]

$$\mathrm{d}F_{\text{NH}(F)}/\mathrm{d}x = \pi \rho R^2 V\, \mathrm{d}w_d/\mathrm{d}x \tag{21}$$

where V is the air speed, and w_d is the local fin-induced downwash. The variation of the downwash along the centerline can be computed from the force distribution on the fins [26], as given by Eq. (16), and we have

$$\begin{aligned} w_d(x) &= V (C_{L\alpha}/C_{l\alpha}) \alpha_F \\ &\quad \times \int_{x_{fs}}^{x_{fe}} \int_R^b [8\pi d(d - x + x_F)]^{-1} \Delta C_{p\alpha}(x_F, s)(1 + R^2/s^2)\, \mathrm{d}s\, \mathrm{d}x_F \end{aligned} \tag{22}$$

where $d = \sqrt{(x - x_F)^2 + s^2}$. Thus, Eq. (21) can be applied to calculate the fin-induced normal force on the hull and the corresponding pitching and yawing moments, which are then added to the right-hand side of Eq. (1).

E. Axial Drag

The axial force is composed of two components, the contributions from the hull and the fins, respectively. At low angles of attack, these forces can be obtained as

$$F_{xH} = -q_0 C_{\text{DH0}} S_H \cos^2 \alpha, \qquad F_{xF} = -q_0 C_{\text{DF0}} S_F \cos^2 \alpha_F \tag{23}$$

where the angle of attack of the hull α is computed from the local velocity at the CV, C_{DH0} and C_{DF0} are the zero-angle axial drag coefficients of the hull and the fins, respectively, and S_H and S_F are the corresponding reference areas. For example, these drag coefficients can be obtained in [21]. To incorporate the axial drag, the forces from Eq. (23) are added to the right-hand side of Eq. (1).

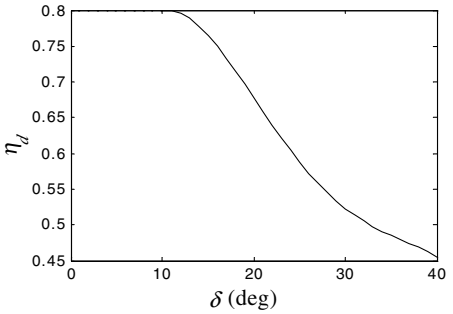

Fig. 10 η_d for plain flap.

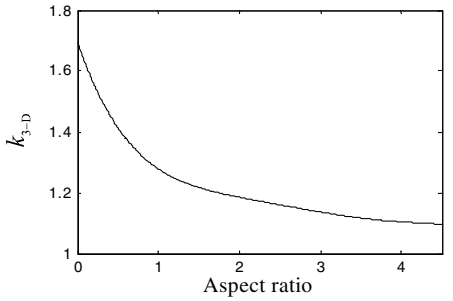

Fig. 11 3-D effectiveness factor ($\tau = 0.5$).

F. Force and Moment Due to Control Surface Deflection

The force and moment due to the control surface deflections also need to be estimated. An estimation method for the effects of flap deflection on the aerodynamics of a 2-D airfoil section is given in [21], and this is now extended to 3-D fins. That is, the lift coefficient from the deflection of the control surface can be computed as

$$\Delta C_L = C_{L\alpha} \tau \eta_d k_{3\text{-D}} \delta \tag{24}$$

where δ is the deflection angle of the control surface. $C_{L\alpha}$ is the 3-D lift curve slope. The theoretical effectiveness factor τ is derived from potential flow theory as [21]

$$\tau = 1 - (\theta_f - \sin \theta_f)/\pi \tag{25}$$

where $\theta_f = \cos^{-1}(2c_f/c - 1)$, in which c_f and c are the flap chord and airfoil chord, respectively. η_d is a correction factor based on experiments and given as a function of the plain flap deflection, shown in Fig. 10. $k_{3\text{-D}}$ is an efficiency factor accounting for 3-D effects, which is a function of τ and the aspect ratio [19]; for example, Fig. 11 shows $k_{3\text{-D}}$ for the case where $\tau = 0.5$.

The increment in the drag coefficient ΔC_D, due to the flap deflection, is given approximately for plain flaps as [21]

$$\Delta C_D = 1.7 (c_f/c)^{1.38} (S_f/S_{\text{FA}}) \sin^2 \delta \tag{26}$$

where S_f and S_{FA} are the flap and fin area, respectively. The influence of flap deflection on the pitching moment coefficient can be estimated from thin airfoil theory, that is, the ratio of $\Delta C_{M1/4}$ to ΔC_L is written as [21]

$$\frac{\Delta C_{M1/4}}{\Delta C_L} = -\frac{2 \sin \theta_f - \sin 2\theta_f}{8(\pi - \theta_f + \sin \theta_f)} \tag{27}$$

where $\Delta C_{M1/4}$ is the pitch moment coefficient about the 1/4 chord.

The forces and moments due to the rudder and elevator deflections can be estimated using Eqs. (24), (26), and (27), and then added to the right-hand side of Eq. (1).

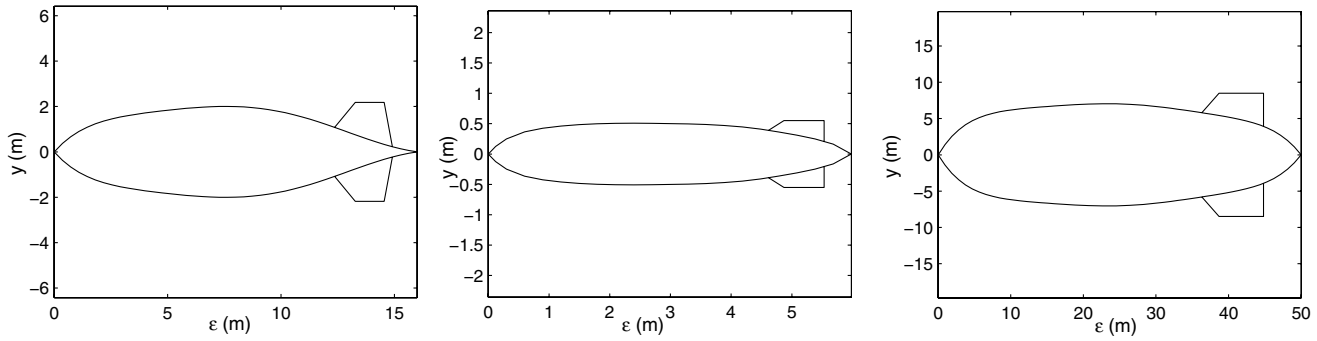

a) The Lotte airship **b) The Akron model** **c) The Skyship-500 airship**

Fig. 12 Profiles of the airships in simulation examples.

V. Linearized Model

A linear dynamics model is now formulated to allow a quantitative assessment of the flight stability and the response to control inputs of the airship. The nonlinear dynamics model developed in Secs. II, III, and IV can be written as a set of first-order ordinary differential equations as

$$\dot{\mathbf{X}} = \mathbf{F}(\mathbf{X}, \mathbf{U}) \tag{28}$$

where $\mathbf{X}$ is the state vector defined as $\mathbf{X} = [u, w, q, \theta, v, p, r, \phi]^T$. The first four states describe the longitudinal motion and the last four describe the lateral motion. $\mathbf{U}$ is the control input vector, such as the elevator and rudder deflections. Equation (28) represents eight nonlinear equations, or $\mathbf{F} = [f_1, f_2, \ldots, f_8]^T$. The time rates of change of the linear and angular velocities contained in $\dot{\mathbf{X}}$ are obtained from Eq. (1), with the aerostatics and aerodynamics models incorporated. In addition, $\dot{\phi}$ and $\dot{\theta}$ can be computed as follows [5]:

$$\dot{\phi} = p + q\sin\phi\tan\theta + r\cos\phi\tan\theta, \qquad \dot{\theta} = q\cos\phi - r\sin\phi \tag{29}$$

To derive the linear dynamics model, the first step is to introduce a reference equilibrium state $\mathbf{X}_e$, about which the system will be linearized, and the corresponding control $\mathbf{U}_e$. If the airship is in steady level flight at equilibrium, then $\mathbf{X}_e = [u_e, 0, 0, 0, 0, 0, 0, 0]^T$, where u_e is an equilibrium speed. The second step is to write the equations for the small disturbance from equilibrium as

$$\Delta\dot{\mathbf{X}} = \mathbf{F}(\mathbf{X}_e + \Delta\mathbf{X}, \mathbf{U}_e + \Delta\mathbf{U}) \approx \mathbf{A}\cdot\Delta\mathbf{X} + \mathbf{B}\cdot\Delta\mathbf{U} \tag{30}$$

where $\mathbf{A} = \partial\mathbf{F}/\partial\mathbf{X}$ is the state matrix, or the Jacobian of $\mathbf{F}$ with respect to $\mathbf{X}$, with a similar definition of the control input matrix $\mathbf{B} = \partial\mathbf{F}/\partial\mathbf{U}$. $\mathbf{A}$ and $\mathbf{B}$ can be numerically evaluated at $\mathbf{X}_e$ and $\mathbf{U}_e$ by a finite difference of the nonlinear differential equations. This method has been previously applied to investigate the stability of a tethered aerostat [27].

Once the matrix $\mathbf{A}$ is obtained, the airship's stability is characterized by the eigenvalues and eigenvectors of $\mathbf{A}$. The eigenvalues can be either as distinct real numbers, representing nonoscillatory modes, or as complex conjugates as $\lambda_{1,2} = \sigma \pm \mathrm{j}\omega_d$, representing oscillatory modes. For an oscillatory mode, the natural frequency and damping ratio can be evaluated from σ and ω_d. For a stable airship, the real parts of all the eigenvalues must be negative. The eigenvector represents the relationship of the elements of the state variables in the corresponding mode. Each element of an eigenvector denotes the magnitude and phase of the response of a particular state variable relative to other states.

VI. Numerical Simulation

The numerical simulation results presented in this section include three parts. First, the added-mass terms and steady-state aerodynamic force estimates are shown and compared to CFD calculation or wind-tunnel test results. Next, the nonlinear dynamics simulation results for the Skyship-500 airship are shown and the responses due to control surface deflection are analyzed. Third, the linear dynamics model of the Skyship-500 airship is analyzed to evaluate the flight stability and the control responses in the frequency domain.

A. Validation of the Aerodynamics Model

1. Added Mass and Moment of Inertia of the Lotte Airship

CFD packages have been developed to compute the aerodynamics of 3-D bodies in potential flow and these have been applied to the added-mass calculation for airships. For example, in [28], a CFD package was applied to compute the added mass and moment of inertia of the Lotte airship, shown in Fig. 12a. This CFD method uses a distribution of source density on the body surface and solves the distribution necessary to meet the boundary conditions. We now use these results to evaluate the estimation method given in Sec. IV.A.2. The CFD results for the added mass and moment of inertia are listed in Table 1 and compared to our estimation results. We can see that the estimation method presented here leads to a reasonable approximation for the added mass of the bare hull and the hull–fin combination. As well, we note that the fins have a considerable effect on the added moment of inertia.

2. Steady-State Aerodynamics of the Akron Airship Model

A great deal of experimental wind-tunnel results on the steady-state aerodynamics can be found in the literature for older rigid airships. In this paper, the experimental results for the Akron airship model [23] (shown in Fig. 12b) are used to test our aerodynamics computation. The measured normal force and pitching moment (about the CV) coefficients at low angles of attack are compared to our estimation results in Figs. 13a and 13b, for both bare hull and hull–fin combinations. We can see that the estimates from Sec. IV can match the experimental results.

B. Nonlinear Dynamic Simulation for the Skyship-500 Airship

A dynamic simulation program has been developed in the MATLAB environment to implement the nonlinear dynamics model discussed in Secs. II, III, and IV. In the numerical simulation, the Skyship-500 airship, shown in Fig. 12c, is used as an example, because the dimensional and inertial parameters and flight test data are available for this airship [7,29]. This subsection presents the simulation results for the responses due to elevator or rudder deflection and compares them to flight test results.

Table 1 Added-mass result

	Bare hull		Hull–fin combination	
Added-mass terms	CFD [28]	Prediction	CFD [28]	Prediction
m_{11}, kg	13	11	12.7	11
m_{22}, kg	112	114	129	125
m_{55}, kg × m^2	759	793	1379	1279

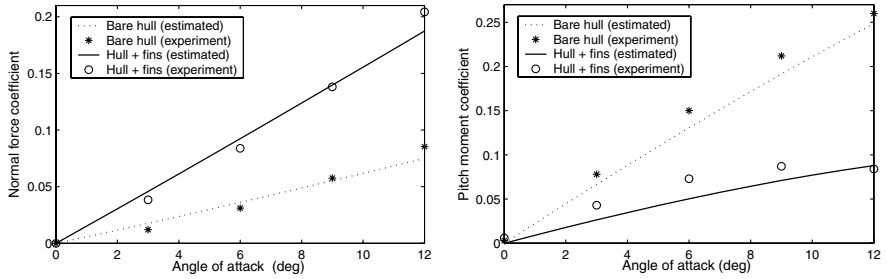

a) Normal force result **b) Pitch moment result**

Fig. 13 Steady-state aerodynamics results of the Akron model.

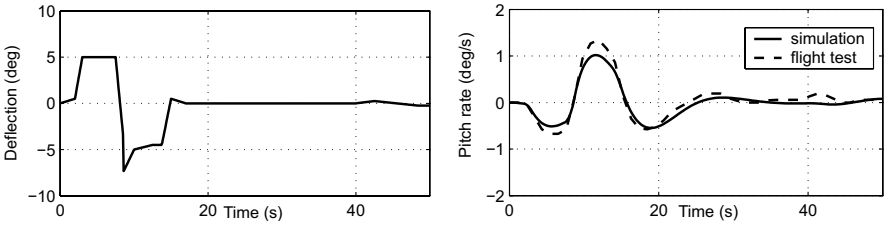

a) Elevator deflection δ_E **b) Time history of pitch rate q**

Fig. 14 Elevator input and response results at 25 kt.

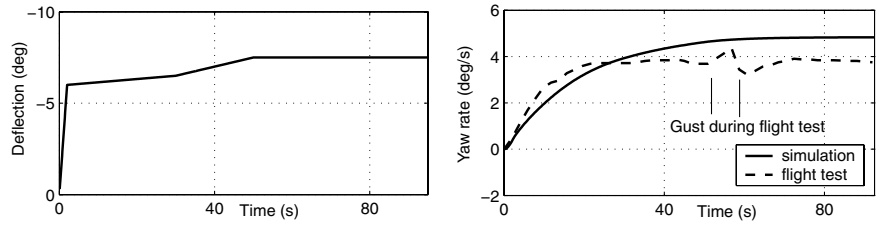

a) Rudder deflection δ_R **b) Time history of yaw rate r**

Fig. 15 Rudder input and response results at 25 kt.

The dimensions, mass, and moment of inertia used in the simulation are obtained from [7,29]. The body frame is located at the CV of the hull. To predict the responses from the dynamic simulation program, some control force and moment are first applied in the simulation so that the airship begins its flight in a trim condition at a constant airspeed of 25 kt.

1. Responses due to Elevator Deflection

In this example, the elevator deflection input δ_E (positive trailing edge downward), shown in Fig. 14a, is obtained from the flight test in [7]. The resulting time histories of the pitch rate from the simulation and the flight test [7] are shown in Fig. 14b, where we find that the simulated response is very close to the flight test data.

2. Responses due to Rudder Deflection

In this example, the steplike rudder input δ_R (positive trailing edge left) is plotted in Fig. 15a, and the response results of the yaw rate are compared to the flight test data [7] in Fig. 15b. A proportional controller is applied to the thrust input so that the airship maintains a constant airspeed. We can see that the predicted steady-state yaw rate is higher than the test data by about 20%, but generally speaking, the dynamic simulation program provides a reasonable match to the major trends in the flight test.

3. Yaw Rate in Steady Turn

A steady rudder deflection leads to a steady turn flight for the airship. In this example, the yaw rates in steady turns are computed for various rudder deflection angles (from −30 to 30 deg) at 25 kt. The simulated results are plotted and compared to the flight test results [29] in Fig. 16. We can see that the turning rate is a nonlinear function of the rudder deflection and this function is reasonably estimated by the dynamics simulation program.

C. Linearized Model and Stability Analysis for the Skyship-500 Airship

1. Control Responses in the Frequency Domain

The nonlinear dynamics model is linearized for the Skyship-500 airship using the approach in Sec. V. It is found that the state matrix **A** can be partitioned into four distinct submatrices as

$$\mathbf{A} = \begin{bmatrix} [\mathbf{A}_{\text{long}}]_{4\times4} & [\mathbf{0}]_{4\times4} \\ [\mathbf{0}]_{4\times4} & [\mathbf{A}_{\text{lat}}]_{4\times4} \end{bmatrix} \tag{31}$$

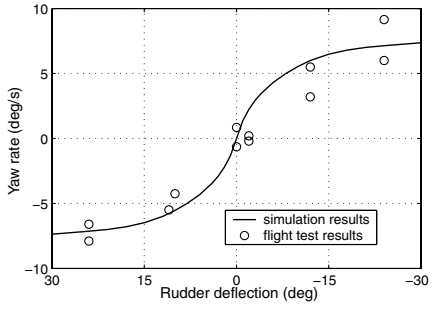

Fig. 16 Yaw rate in steady turn (at 25 kt).

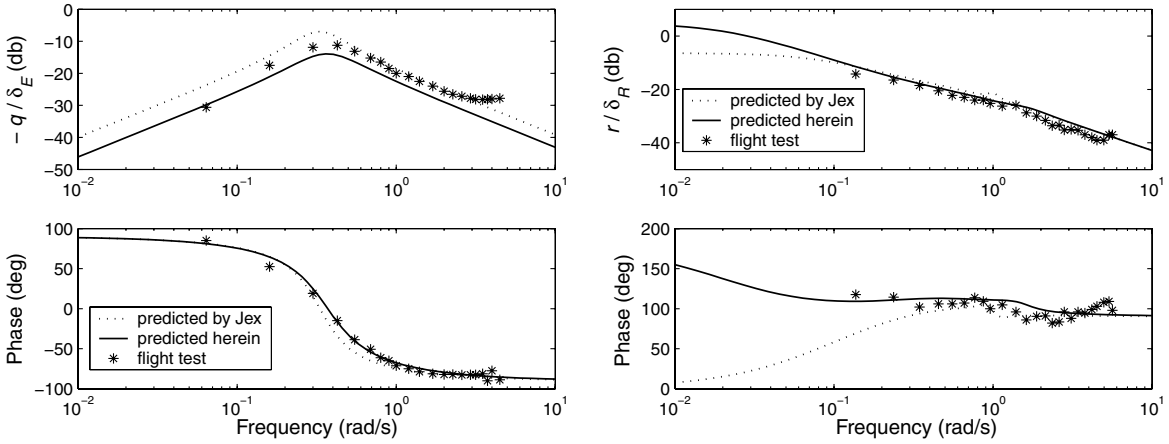

a) Pitch rate response due to elevator input **b) Yaw rate response due to rudder input**

Fig. 17 Control response in the frequency domain at 25 kt.

where all elements in the lower left submatrix are zero, while some in the upper right submatrix are not exactly zero but of much smaller magnitude than the elements in $[\mathbf{A}_{\text{long}}]$ and $[\mathbf{A}_{\text{lat}}]$. Therefore the longitudinal and lateral motions are essentially decoupled.

Once the matrices **A** and **B** are obtained, the control responses in the frequency domain can be computed. The responses due to elevator and rudder inputs are displayed in Bode plots in Figs. 17 and 18 for forward speeds u_e of 25 and 40 kt, respectively. The responses predicted herein are compared to the flight test results and the model prediction of Jex [7]. The linear model presented herein provides a good match to the major trends in the flight test and provides more accurate predictions than Jex's model results for the yaw rate phase angle response at low frequencies.

2. *Stability and Natural Modes*

The eigenvalues and eigenvectors of $[\mathbf{A}_{\text{long}}]$ and $[\mathbf{A}_{\text{lat}}]$ for the Skyship-500 airship are investigated as they change with the variations in the equilibrium speed from 0 to 30 m/s.

The first two longitudinal modes have negative real eigenvalues, whose magnitude increases with speed (i.e., they become more stable) as shown in Fig. 19a. The eigenvalues of the third longitudinal mode are a complex conjugate pair and the corresponding natural frequency and damping ratio are plotted in Fig. 19b. The eigenvectors are then studied to obtain the relative values (magnitude and phase) between the different state variables of each mode, using the following steps. First, nondimensionalize each component of the eigenvector, that is, each linear velocity component $(\Delta u, \Delta v, \Delta w)$ is divided by the equilibrium speed u_e, each angular velocity component $(\Delta p, \Delta q, \Delta r)$ is divided by $u_e/(V_B)^{1/3}$, and the rotation components $\Delta\theta$ and $\Delta\phi$ are not modified. Second, select a reference state variable and factor the eigenvector to make this state equal to unity. Third, plot all the real and imaginary parts of each component in an Argand diagram. For eigenvalues with complex conjugates $\lambda_{1,2} = \sigma \pm j\omega_d$, only the eigenvector corresponding to $\sigma + j\omega_d$ is plotted. For example, the vector diagrams of the longitudinal modes at 40 kt are shown in Fig. 20.

The motion characteristics of each longitudinal mode at different speeds have similar trends to the mode results of another airship in [11] and can be described as follows:

1) The first longitudinal mode is a surge subsidence mode caused by the axial aerodynamic drag and can be considered as a 1-DOF motion in forward velocity Δu. The modes are neutrally stable at zero speed and become more stable as the speed increases.

2) The second longitudinal mode is a heave–pitch subsidence mode caused by the transverse aerodynamic drag. The dominant motion is Δw near zero speed, coupling with some $\Delta\theta$, Δq, and Δu as the speed increases to about 12 m/s. The pitch rate generates an additional aerodynamic damping moment, thus further stabilizing this mode.

3) The third longitudinal mode is a pitch–incidence oscillation mode. Near zero speed, the dominant motion is the pitch rate Δq, combined with some Δu. As the speed increases to about 14 m/s, Δw becomes apparent and the incidence causes a Munk moment,

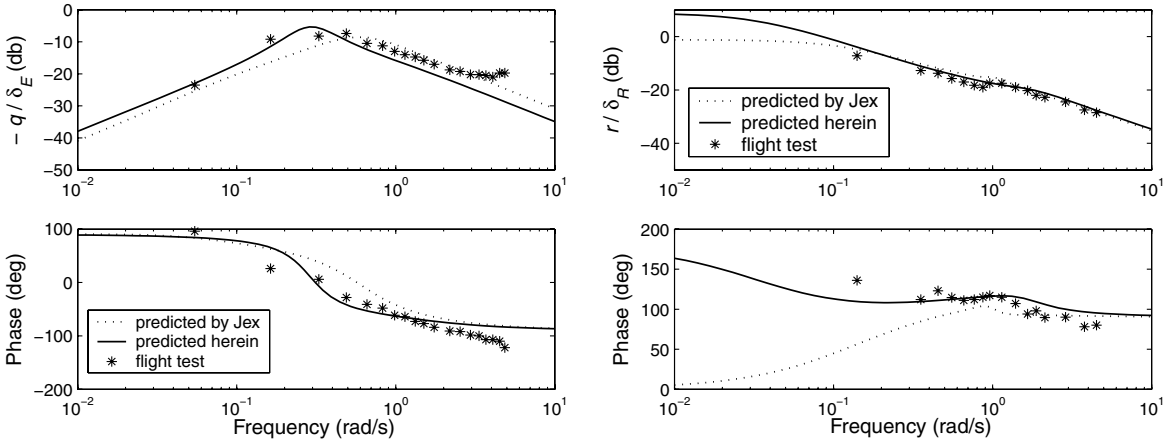

a) Pitch rate response due to elevator input **b) Yaw rate response due to rudder input**

Fig. 18 Control response in the frequency domain at 40 kt.

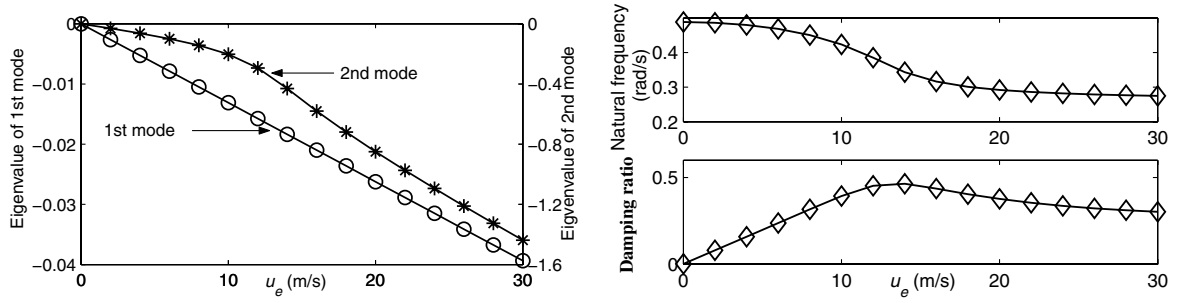

a) Longitudinal modes (1st and 2nd) b) Longitudinal mode (3rd)

Fig. 19 Longitudinal modes.

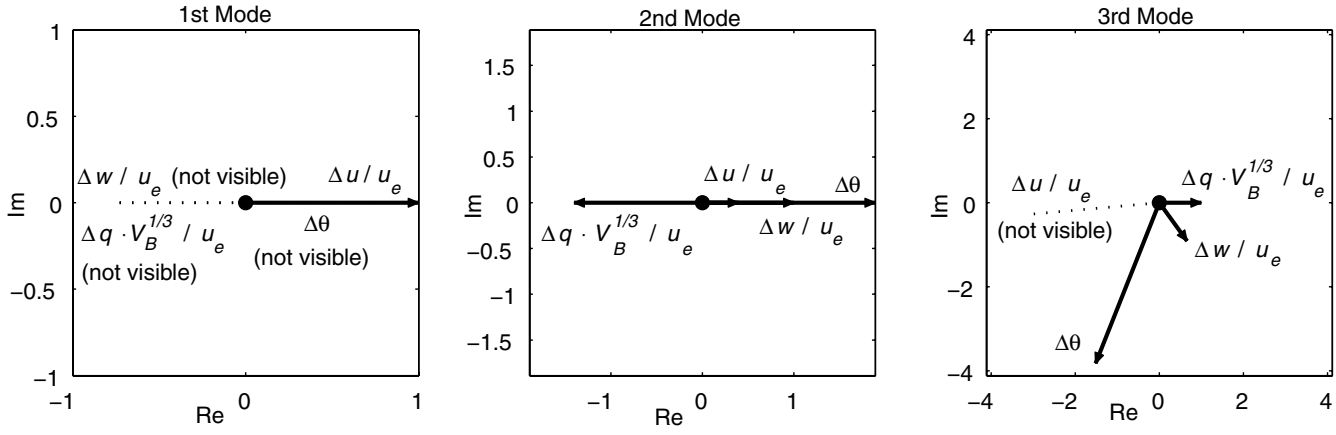

Fig. 20 Vector diagram of longitudinal modes at 40 kt.

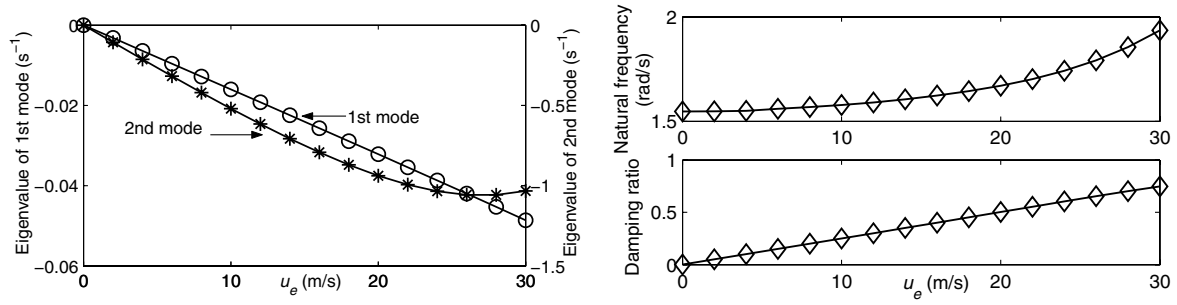

a) Lateral modes (1st and 2nd) b) Lateral mode (3rd)

Fig. 21 Lateral modes.

which tends to destabilize the system, thereby leading to a decrease in the damping ratio at speeds from 14 m/s to 30 m/s.

The lateral stability modes can be studied using a similar approach. The first two lateral modes have negative real eigenvalues as shown in Fig. 21a. The eigenvalues of the third lateral mode are a complex conjugate pair and the corresponding natural frequency and damping ratio are plotted in Fig. 21b. The motion characteristics of each lateral mode can be described as follows:

1) The first lateral mode is a sideslip-yaw subsidence mode. Near zero speed, the most apparent motion is Δv, coupling with some yaw rate Δr. As the speed increases, the roll rotation $\Delta\phi$ becomes apparent because of the centrifugal force.

2) The second lateral mode is a yaw–roll subsidence mode. The yaw rate Δr couples with Δv at near-zero speed. This mode becomes slightly less stable as the speed increases from 25 m/s to 30 m/s. This is likely due to the unstable effect of the Munk moment, as in the longitudinal mode analysis.

3) The third lateral mode is a roll oscillation mode, coupling with some Δv, and with some Δr at high speed. The damping ratio curve shows that the aerodynamic damping becomes increasingly significant as the speed increases.

VII. Conclusions

A modeling procedure for the nonlinear dynamics simulation of airships is presented. Estimation methods are provided for various aerodynamic effects, and then verified by comparing to CFD or wind-tunnel experimental results. A simulation program is developed from the dynamics model, which can reasonably predict the transient response and flight behavior for the Skyship-500 airship, based on a comparison to flight test data.

The linear equations of motion can be obtained from the nonlinear dynamics model using a finite difference approach. The resulting linear model for the Skyship-500 decouples into longitudinal and lateral subsets. The control responses in the frequency domain due to control surface deflections are a good match to the flight test results. The stability of the airship is then analyzed at various speeds. At zero speed, all modes of motion are neutrally stable. The stability

improves with increasing speed for all modes with the exception of the third longitudinal mode and the second lateral mode. The stability of these two modes increases with increasing speed until a certain point after which the stability decreases slightly.

With the trust gained from validation, the dynamics model and simulation program can be used to evaluate the flight and control performance of other airships.

References

[1] Khoury, G., and Gillett, J., *Airship Technology*, Cambridge Univ. Press, Cambridge, U.K., 1999, pp. 5–24, 73–106.

[2] Elfes, A., Bueno, S., Bergerman, M., and Ramos, J. G., "A Semi-Autonomous Robotics Airship for Environmental Monitoring Missions," *Proceedings of the IEEE International Conference on Robotics and Automation*, Vol. 4, IEEE, Piscataway, NJ, May 1998, pp. 3449–3455.

[3] Kulczycki, E. A., Joshi, S. S., Hess, R. A., and Elfes, A., "Towards Controller Design for Autonomous Airship Using SLC and LQR Methods," *AIAA Guidance, Navigation and Control Conference and Exhibit*, AIAA, Reston, VA, 21–24 Aug. 2006.

[4] Schmidt, D. K., "Dynamic Modeling, Control and Station-Keeping Guidance of a Large High-Altitude 'Near-Space' Airship," *AIAA Guidance, Navigation and Control Conference and Exhibit*, AIAA, Reston, VA, 21–24 Aug. 2006.

[5] Etkin, B., *Dynamics of Flight: Stability & Control*, 3rd ed., Wiley, New York, 1996, pp. 93–104.

[6] Tischler, M. B., Ringland, R. R., and Jex, H. R., "Heavy Airship Dynamics," *Journal of Aircraft*, Vol. 20, No. 5, 1983, pp. 425–433.

[7] Jex, H. R., and Gelhausen, P., "Pre- and Post-Flight-Test Models Versus Measured Skyship-500 Control Responses," *7th AIAA Lighter-Than-Air Technology Conference*, AIAA, New York, 17–19 Aug. 1987, pp. 87–97.

[8] Amann, J. H., "A Comparison of a Nonlinear Flight Dynamic Simulation of an Airship with Flight Test Results," *7th AIAA Lighter-Than-Air Technology Conference*, AIAA, New York, 17–19 Aug. 1987, pp. 78–86.

[9] Jones, S. P., and DeLaurier, J. D., "Aerodynamic Estimation Techniques for Aerostats and Airships," *Journal of Aircraft*, Vol. 20, No. 2, 1983, pp. 120–126.

[10] Azinheira, J. R., de Paiva, E. C., and Bueno, S. S., "Influence of Wind Speed on Airship Dynamics," *Journal of Guidance, Control, and Dynamics*, Vol. 25, No. 6, 2002, pp. 1116–1124.

[11] Cook, M. V., Lipscombe, J. M., and Goineau, F., "Analysis of the Stability Modes of the Non-Rigid Airship," *The Aeronautical Journal*, Vol. 104, No. 1036, 2000, pp. 279–290.

[12] Fossen, T. I., *Guidance and Control of Ocean Vehicles*, Wiley, New York, 1998, pp. 5–42.

[13] Lamb, H., *Hydrodynamics*, 6th ed., Dover, New York, 1945, pp. 160–201.

[14] Newman, J. N., *Marine Hydrodynamics*, MIT Press, Cambridge, MA, 1977, pp. 132–149.

[15] Munk, M. M., "The Aerodynamic Forces on Airship Hulls," NACA TR-184, 1924.

[16] Nielsen, J. N., *Missile Aerodynamics*, AIAA, Cambridge, MA, 1988, pp. 363–394.

[17] Blevins, R. D., *Formulas for Natural Frequency and Mode Shape*, Krieger, New York, 1979, p. 405.

[18] Meyerho, W. K., "Added Masses of Thin Rectangular Plates Calculated from Potential Theory," *Journal of Ship Research*, Vol. 14, No. 2, 1970, pp. 100–111.

[19] Finck, R. D., USAF Stability and Control DATCOM, Flight Control Division, Air Force Dynamics Laboratory, Wright–Patterson Air Force Base, OH, 1978, Secs. 4.1, 4.2, and 6.1.4.

[20] Hopkins, E. J., "A Semi-Empirical Method for Calculating the Pitching Moment of Bodies of Revolution at Low Mach Numbers," NACA RM-A51C14, 1951.

[21] McCormick, B. W., *Aerodynamics, Aeronautics and Flight Mechanics*, 2nd ed., Wiley, New York, 1995, pp. 99–116, 160–165.

[22] Pitts, W. C., Nielsen, J. N., and Kaattari, G. E., "Lift and Center of Pressure of Wing-Body-Tail Combinations at Subsonic, Transonic and Supersonic Speeds," NACA TR-1307, 1957.

[23] Freeman, H. B., "Force Measurements on a 1/40-Scale Model of the U.S. Airship Akron," NACA TR-432, 1932.

[24] Freeman, H. B., "Pressure Distribution Measurements on the Hull and Fins of a 1/40-Scale Model of the U.S. Airship Akron," NACA TR-443, 1933.

[25] Lawrence, H. R., and Flax, A. H., "Wing-Body Interference at Subsonic and Supersonic Speeds—Survey and New Developments," *Journal of the Aeronautical Sciences*, Vol. 21, No. 5, 1954, pp. 289–324.

[26] von Karman, T., and Burgers, J. M., "General Aerodynamic Theory—Perfect Fluids," *Aerodynamic Theory*, edited by W. F. Durand, Vol. 2, Dover, New York, 1943, p. 153.

[27] Lambert, C., and Nahon, M., "Stability Analysis of a Tethered Aerostat," *Journal of Aircraft*, Vol. 40, No. 4, 2003, pp. 705–715.

[28] Lutz, T., Fund, P., Jakobi, A., and Wagner, S., "Summary of Aerodynamic Studies on the Lotte Airship," *Proceeding of the 4th International Airship Convention and Exhibition*, Airship Association, Folkestone, U.K., 28–31 July 2002.

[29] Jex, H. R., and Gelhausen, P., "Control Response Measurements of the Skyship-500 Airship," *6th AIAA Lighter-Than-Air Technology Conference*, AIAA, New York, 26–28 June 1985, pp. 130–141.